Tracking Large Anterior Mitral Leaflet Displacements by Incorporating Optical Flow in an Active Contours Framework

Malik Saad Sultan[1] Nelson Martins[1,2] Eva Costa[2] Diana Veiga[2] Manuel João Ferreira[2,3] Sandra Mattos[4] Miguel Tavares Coimbra[1]

***Abstract*— Echocardiography is an important tool to detect early evidence of mitral valve degradation associated with rheumatic heart disease. The segmentation and tracking of the Anterior Mitral Leaflet helps to quantify the morphologic valve anomalies, such as the leaflet thickening, shape and the mobility changes. The tracking of this leaflet throughout the cardiac cycle is still an open challenge in the research community. The widely used active contours segmentation framework fails when faced with large leaflet displacement. In this work, we propose the integration of optical flow in an open-ended active contour framework to address this difficulty. This additional information promotes solutions with contours next to high leaflet displacements, resulting in superior performance. The algorithm was tested on 9 fully annotated real clinical videos, acquired from the parasternal long axis view. The algorithm is compared with our previous work. Results show a clear improvement in situations where the leaflet exhibits large displacement or irregular shapes, with an average error of 4.5 pixels and a standard deviation of 2 pixels.**

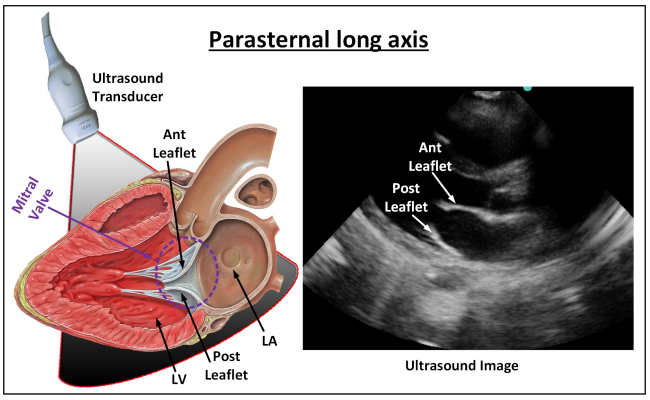

Fig. 1. Parasternal long axis view (adapted from [10]) of a normal mitral valve in diastole.

I. Introduction

Rheumatic heart disease (RHD), among other causes, can be a serious consequence of repeated episodes of acute rheumatic fever (ARF). RHD is still a major problem in developing countries, affecting about 15 million people worldwide. The disease is responsible for 233,000 deaths per year, with 282,000 new registered cases [1]. Echocardiography has proven to be very sensitive in detecting early RHD cases, even without access to the patients additional clinical information [2]. Echocardiography screening has played a vital role to identify the cases with RHD and to define the disease burden, in developing countries [3].

The mitral valve is the most commonly affected heart valve by RHD, with or without the involvement of the other valves [2]. The parasternal long axis ($PLAX$) is the best window to analyze the mitral valve (Fig. 1) [4]. This view allows the evaluation of the thickness, shape and the motion pattern of the mitral leaflets that are key features to identify RHD cases. The manual evaluation and quantification is time consuming, expensive and subjective. To measure and quantify such features, we need a robust segmentation and tracking framework that can automatically delineate the anatomical structures in the image.

The active contour framework [5] is widely used by the research community to segment and track the structures in medical images/videos. They are the parametric contours that deform under the image characteristics and other shape constraints.

This method has several limitations such as high dependency on the initial contour placement or high sensitivity to edge and noise information. The research community has addressed some of these problems, by introducing improvements such as pressure force (balloon) [6] and gradient vector flow [7].

The segmentation and tracking of the mitral leaflets in ultrasound was addressed in previous works [8 - 11]. Based on the fact that the motion of the cardiac muscles are different from the mitral leaflet, two active contours segments were used and are initialized by the rough segmentation obtained through the curve fitting algorithm [8]. Optical flow is used to obtain the initial boundaries that are then refined by the active contours [9]. The motion of the mitral leaflet is very irregular, it rotates, translates and shows large leaflet displacement and thus proposed approach fails in those situations. The internal and external energy of the classical snake model is modified to obtain robust tracking of the anterior mitral leaflet (AML) [10]. Open-ended active contours were used and the external energy of the model was adapted to encourage the end point of the contour to continually follow the tip of the AML. However, the proposed approach fails in situations when the AML shows large displacement. Another approach is based on the outlier detection of a low rank matrix to track the AML in ultrasound [11]. The algorithm is fully automatic and unsupervised. However, it requires parameter adjustment, and is very sensitive to noise

[1]Instituto de Telecomunicações, Faculdade de Ciências da Universidade do Porto, Portugal
[2]Enermeter, Sistemas de Medição, Lda, Braga, Portugal
[3]Centro Algoritmi, University of Minho, Guimarães, Portugal
[4]Círculo do Coração de Pernambuco, Recife PE, Brazil

978-1-5090-2809-2/17/$31.00 ©2017 IEEE

and the chosen matrix rank. In a nutshell, current state-of-the-art approaches fail in situations when the mitral leaflet exhibit large displacements and are unable to recover from these failures.

In this work, our main objective is to improve the performance of the segmentation and tracking algorithm by addressing situations with large displacements. As contributions, our external energy is modified to incorporate optical flow energy, promoting solutions associated with the large motion exhibited by the mitral valve leaflet. This work builds upon our previous research [10] that frequently encounters failure in such situations.

This paper is organized as follows. Section 2 provides the overview of the classical snake model. Section 3 presents the details of improved snake model. Section 4 reports the tracking results of the AML and finally section 5 concludes the paper with a discussion and future work.

II. Classical Snake

The active contour model, also known as snakes, uses parametric curves $V(S) = (x(S), y(S))^T \; S \in [0,1]$ that deform under the image force, limited by shape constraints. The total energy of the snake model consist of a combination of internal and external energy.(1).

$$\int_0^1 \left(\overbrace{\frac{1}{2}\left[\underbrace{\alpha \left\| \frac{\partial V}{\partial S} \right\|^2}_{Elasticity} + \underbrace{\beta \left\| \frac{\partial^2 V}{\partial S^2} \right\|^2}_{Stiffness} \right]}^{Internal} + \overbrace{E_{ext}(V)}^{External} \right) ds \quad (1)$$

The internal energy is responsible to maintain the predefined elasticity and the stiffness of the parametric curve. The parameters α and β allow us to control the elastic force and the bending force, respectively. The external energy is derived from the image and thus attracts the contour towards the edges (local minima), intensity (bright structures), or other visual features extracted.

Searching for a solution implies transforming the problem into an energy minimization one. The Euler Lagrange is typically applied, giving us the final equation of the snake model (2).

$$\alpha \frac{\partial^2 V}{\partial S^2} - \beta \frac{\partial^4 V}{\partial S^4} - \nabla E_{ext.} = 0 \quad (2)$$

III. Improved Snake Model

The focus of this work is to improve the tracking capabilities of our previous algorithm [10]. We assume perfect segmentation in the very first frame, which is then tracked throughout the cardiac cycle. Since this is an extension of our previous work, the integration of the optical flow in classical snake model is here explained in more detail.

A. Internal energy

In this work, we used the open ended contours obtained through the free boundary condition. The open ended contours results into lines that segment and track the AML in a more natural way. The end points are free to move on the image to get an energy minimum and are constrained to stay close to their neighbors [10]. The elasticity and stiffness are controlled in the same way as in the classical snake model [5].

B. External energy

The external energy is divided into two main parts, the image and the motion energy (3).

$$E_{ext.} = E_{image} + E_{motion} \quad (3)$$

The image energy is the same used in our previous work (4) [10], consisting of three terms, the line and the edge energy obtained through the Difference of Gaussian, and the Harris corner energy [12]. The Harris corner energy encourages the endpoint of the contour to continuously follow the tip of the AML.

$$\begin{aligned} E_{image} = w_{harris} E_{harris} - w_{DoG\_line} E_{DoG\_line} \\ + w_{DoG\_edge} E_{DoG\_edge} \end{aligned} \quad (4)$$

The motion energy quantifies the image displacement energy for overcoming the limitation (tracking failure in large motion) of our previous work. Optical flow is integrated in the external energy of the classical snake model as a dynamic energy (5).

$$E_{motion} = w_{optical\_flow} E_{optical\_flow} \quad (5)$$

Optical flow methods, which attempt to quantify the motion of brightness patterns in a sequence of images, can be divided into local methods, such as Lucas-Kanade [13, 14], global methods, such as Horn-Schunck [15]. We selected the Lucas-Kanade approach, considered by literature as still the most interesting cost-benefit optical flow method [16].

In this work, we used a coarse-to-fine approach to Lucas-Kanade to efficiently handle both large and small motion. This consists on creating multiple copies of the same image with different resolutions. In each level, the resolution is reduced $1/4$ of the size of the previous level (6).

$$\begin{aligned} g_L(x,y) = \\ \sum_{m=-2}^{2} \sum_{n=-2}^{2} w(m,n)\, g_{L-1}(2x+m, 2y+n) \end{aligned} \quad (6)$$

The 2D mask w of size 5×5 is convolved with the image g at level $L-1$, to obtain the low resolution image at level L. The pre-filtering step in pyramid construction plays a vital role for the true optical flow estimation [17]. Based on this work, a Gaussian filter with the standard deviation of 1.3

is used to smooth the image for all the levels instead of smoothing only the initial image. The image is downsampled using the nearest neighbor approach with a scale factor of 0.5.

The pipeline to obtaining the true optical flow in this pyramid approach is as follows. First, the optical flow is computed in the highest level ($L3$). Since the motion is reduced in the highest level ($L3$) due to low resolution, the estimated optical flow is easier to calculate given more image structures. The obtained flow in previous level ($L3$) is used as an initial guess to obtain the flow in the next level ($L2$). This level ($L2$) should be double the resolution of the last level ($L3$). Thus, we used the bilinear interpolation to obtain the optical flow in that level.

At this point, we have the motion vectors for each pixels that give us the displacement in relation to the previous frame (Fig. 2). Our objective is to integrate this information (displacement and direction) in the classical snake model. We added the motion vectors as the displacement force in an external energy that pushes the contour points towards the true image energy, until trapped in local minimum. In simple words, the optical flow is used as a displacement force that pushes the curve towards the local minimum.

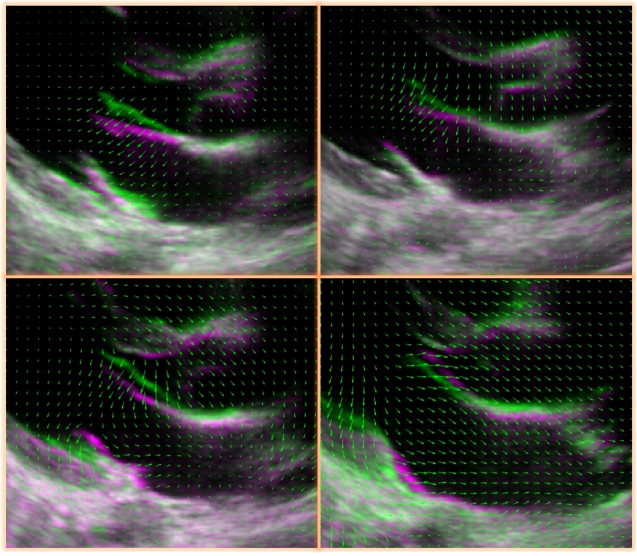

Fig. 2. Motion vectors of the optical flow (Lucas-Kanade). Last frame: Green, Present frame: Magenta

The iterative form of the modified classical snake model is shown (6, 7)

$$\nabla E_{ext.} = \begin{bmatrix} \frac{\partial E_{image}}{\partial x} \\ \frac{\partial E_{image}}{\partial y} \end{bmatrix} + \begin{bmatrix} \frac{\partial E_{motion}}{\partial u} \\ \frac{\partial E_{motion}}{\partial v} \end{bmatrix} = \begin{bmatrix} f_x \\ f_y \end{bmatrix} + \begin{bmatrix} f_u \\ f_v \end{bmatrix} \quad (7)$$

$$\begin{aligned} X_t = \quad & (A+\gamma I)^{-1}(\gamma X_{t-1} - f_x(X_{t-1}, Y_{t-1}) \\ & + f_u(X_{t-1}, Y_{t-1}) \\ Y_t = \quad & (A+\gamma I)^{-1}(\gamma Y_{t-1} - f_y(X_{t-1}, Y_{t-1}) \\ & + f_v(X_{t-1}, Y_{t-1}) \end{aligned} \quad (8)$$

Whereas, I is the identity matrix, γ is the step size and A is coefficient matrix. The first part of the equation $(A+\gamma I)^{-1}$ imposes the internal constraints and the other part attracts the contour toward the image energy.

IV. Results

A. Materials

In one of the activities of Real Hospital Português, in Recife, Brazil, a dataset of ultrasound mitral valve videos ($PLAX$ view) has been collected for the purposes of screening acute rheumatic fever in children. The data was collected using a M-Turbo model by SonoSite ultrasound system, with $C11x$ transducer (5-8 MHz). Nine of these exams were fully annotated (manual segmentation of all frames) using support software and were used to test the novel algorithm proposed in this work. These nine videos include a total of 1137 frames with dimensions of $[351 \times 441]$.

B. Tracking results

The tracking starts with the manual initialization by inserting 6 points on the AML, in the first frame of each video. To evaluate the performance, results of the reference approach [10] and the proposed approach are compared with the ground truth (doctors annotation). The Modified Hausdorff Distance (MHD) [18] error is computed for the ground truth and the automatic segmentation. Table 1 shows the mean, median and the standard deviation of the MHD error in each video, for both the reference and our approach. The results are computed for the most difficult situation, when the AML shows large displacement, for example, at first opening of the AML and in the diastole phase. The results shows improvement in each video, with the overall mean, median and standard deviation of 2, 4.5 and 4.2 pixels, respectively.

TABLE I
TRACKING RESULTS (IN PIXELS)

	Our Approach	**Ref. Approach [10]**
Video No.	STD / Mean / Median	STD / Mean / Median
1	2.2 / 3.2 / 2.5	3.2 / 6.0 / 5.8
2	2.5 / 6.0 / 5.5	4.0 / 9.9 / 11.3
3	1.7 / 4.2 / 3.9	2.5 / 5.8 / 5.3
4	2.2 / 4.9 / 4.5	1.4 / 5.6 / 5.1
5	1.6 / 4.5 / 4.6	2.7 / 6.4 / 5.7
6	3.4 / 5.3 / 4.9	6.2 / 7.9 / 5.3
7	0.7 / 4.7 / 4.6	1.1 / 5.1 / 4.7
8	0.9 / 3.5 / 3.6	0.9 / 4.8 / 4.8
9	3.2 / 4.5 / 3.7	3.5 / 5.4 / 4.2
Total	**2.0 / 4.5 / 4.2**	**2.8 / 6.3 / 5.8**

In order to visually inspect these results, we plotted in the same image the reference approach (green) [10], our approach (blue) and the ground truth (red) (Fig. 3). The Figure 3 clearly shows the limitation of the reference approach. In the case of large leaflet motion there is no force near the contour points that makes the curve evolve towards true boundaries. However, in our proposed approach the optical flow (motion vector) can guide the contour towards true

boundaries. One can see that the results of our approach is approximately overlapping the ground truth, reinforcing the number presented in Table I.

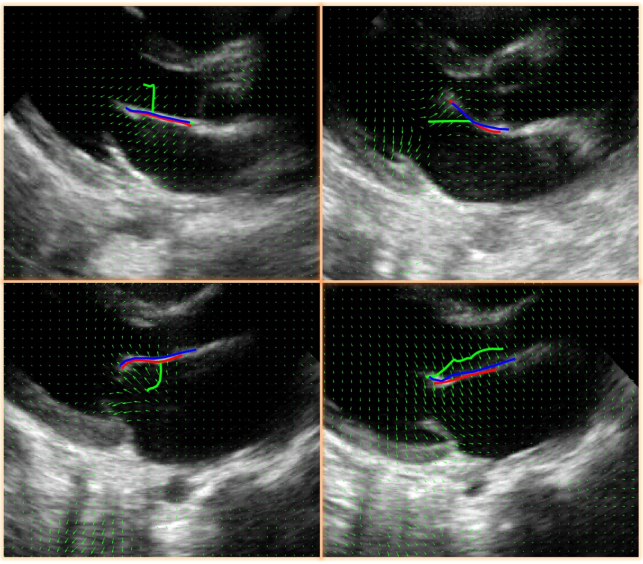

Fig. 3. Tracking of the AML. Red: Ground truth, Green: Ref. approach, Blue: Our approach, Green arrows: Motion vectors

Better tracking performance is achieved but at the cost of computational complexity. The reference algorithm [10] consumes about 0.58 second/frame to automatically delineate the AML. However, our approach takes about 14.07 second/frame.

V. Discussion and Future Work

Experiments showed that the proposed algorithm is more robust than the previous reference, exhibiting improved tracking capability (less failures). The AML shows large displacements and thus classical snake models are not adequate for tracking in such situations, since there is no force that can attract the contour towards the desired location. To overcome this problem, we integrated the optical flow as an external energy in the classical snake framework. The proposed framework considers the movement of tissues in the successive frames for improved tracking performance.

As still unaddressed issues, the proposed algorithm still needs a failure recovery mechanism, and is computationally expensive (due to integration of the optical flow) for portable systems, unless some sort of cloud-based processing is used. These issues will be address in our future work.

Acknowledgement

This article is a result of the project (NORTE-01-0247-FEDER-003507-RHDecho), co-funded by Norte Portugal Regional Operational Programme (NORTE 2020), under the PORTUGAL 2020 Partnership Agreement, through the European Regional Development Fund (ERDF). This work also had the collaboration of the Fundação para a Ciência a e Tecnologia (FCT) grant no: PD/BD/105761/2014 and has contributions from the project NanoSTIMA, NORTE-01-0145-FEDER-000016, supported by Norte Portugal Regional Operational Programme (NORTE 2020), through Portugal 2020 and the European Regional Development Fund (ERDF).

References

[1] Carapetis JR, Steer AC, Mulholland EK, Weber M. The global burden of group A streptococcal diseases. Lancet Infect Dis. 2005;5:685694

[2] B. Remnyi, N. Wilson, A. Steer, B. Ferreira, J. Kado, K. Kumar, J. Lawrenson, G. Maguire, E. Marijon et. al. Feb 2012. World Heart Federation criteria for echocardiographic diagnosis of rheumatic heart diseasean evidence-based guideline, Nat Rev Cardiol. Vol 9, issue 5, pp 297-309

[3] Marijon E, Ou P, Celermajer DS, et al. Prevalence of rheumatic heart disease detected by echocardiographic screening. N Engl J Med. 2007;357:470476.

[4] A.S. Omran, A.A. Arifi, A.A. Mohamed, Echocardiography of the mitral valve, Journal of the Saudi Heart Association, vol. 22, no. 3, pp. 165170, Feb. 2010

[5] Kass M., Witkin A., and Terzopoulos D., Snakes: Active contour models, Int. J. Comput. Vis. 1, 321331 (1988).

[6] L. D. Cohen, On active contour models and balloons, CVGIP: Image Understanding, vol. 53, no. 2, pp. 211218, 1991

[7] C. Xu and J. Prince. Gradient Vector Flow: A new External Force for Snakes. In CVPR, pages 6671, Puerto Rico, USA, 1997

[8] S. Martin, V. Daanen, O. Chavanon, J. Troccaz. Fast Segmentation of the Mitral Valve Leaflet in Echocardiography. Computer Vision Approaches to Medical Image Analysis, Vol. 4241, pp 225-235, 2006

[9] I. Mikic, S. Krucinski, J. D. Thomas. Segmentation and Tracking in Echocardiographic Sequences: Active Contours Guided by Optical Flow Estimates. IEEE transactions on medical imaging, vol- 17, no. 2, April 1998

[10] M. S. Sultan, N. Martins, D. Veiga, M. J. Ferreira, M. T. Coimbra, Tracking of the Anterior Mitral Leaflet in Echocardiographic Sequences using Active Contours, EMBC, 1074-1077, 2016

[11] X. Zhou, C. Yang, W. Yu, Automatic Mitral Leaflet Tracking in Echocardiography by Outlier Detection in the Low-rank Representation, IEEE Conference on Computer Vision and Pattern Recognition, IEEE Computer Society Washington, DC, USA, 972-979, 2012

[12] C. Harris, M. Stephens, A combined corner and edge detector, Alvey vision Conf., 1988

[13] Lucas, B. and Kanade, T. 1981. An iterative image registration technique with an application to stereo vision. In Proc. Seventh International Joint Conference on Artificial Intelligence, Vancouver, Canada, pp. 674679.

[14] Lucas, B.D. 1984. Generalized image matching by the method of differences. PhD thesis, School of Computer Science, CarnegieMellon University, Pittsburgh, PA.

[15] Horn, B. and Schunck, B. 1981. Determining optical flow. Artificial Intelligence, 17:185203.

[16] J.L. Barron, D.J. Fleet, S.S. Beauchemin, Systems and Experiment Performance of Optical Flow Techniques, International Journal of Computer Vision, 12:1, 43-77 (1994)

[17] Sharmin, N., Brad, R. (2012). Optimal Filter Estimation for Lucas-Kanade Optical Flow. Sensors (Basel, Switzerland), 12(9), 1269412709. http://doi.org/10.3390/s120912694

[18] M.-P. Dubuisson, A. K. Jain, 1994. A Modified Hausdorff Distance for Object Matching, Proc, international conference on pattern recognition, Jerusalem, Israel, pp 566-568